Application of Non-Uniform Sampling to Avoid Aliasing in the Precipitation Doppler Spectrum

Syed Mohamed, S. A.K.; Dash, Tworit; Krasnov, Oleg A.; Bout, Jelle; Van Der Meer, Rob; Yarovoy, Alexander G.

Publication date
2024

Document Version
Final published version

Published in
2024 International Radar Symposium, IRS 2024

Citation (APA)
Syed Mohamed, S. A. K., Dash, T., Krasnov, O. A., Bout, J., Van Der Meer, R., & Yarovoy, A. G. (2024). Application of Non-Uniform Sampling to Avoid Aliasing in the Precipitation Doppler Spectrum. In *2024 International Radar Symposium, IRS 2024* (pp. 216-221). (Proceedings International Radar Symposium). IEEE.

Application of non-uniform sampling to avoid aliasing in the precipitation Doppler spectrum

S.A.K Syed Mohamed
Robin Radar Systems, NL
sultan.abdul@robinradar.com

Tworit Dash
Microelectronics, TU Delft
t.k.dash@tudelft.nl

Oleg A. Krasnov
Microelectronics, TU Delft
o.a.krasnov@tudelft.nl

Jelle Bout
Robin Radar Systems, NL
jellebout@live.nl

Rob van der Meer
Robin Radar Systems, NL
rob.vandermeer@robinradar.com

Alexander G. Yarovoy
Microelectronics, TU Delft
a.yarovoy@tudelft.nl

***Abstract*—The problem of aliasing in precipitation Doppler spectrum with uniform pulse repetition time is addressed. This work focuses on de-aliasing such Doppler spectra using non-uniform sampling techniques, namely, Log-periodic and Periodic non-uniform sampling. These techniques reduce the ambiguous main lobes caused by aliasing (by going beyond the observable frequency limit) into ambiguous sidelobes that are distinguishable from the original spectra. The SNR is further enhanced by using an Iterative Adaptive Approach (IAA) algorithm. The performance of Doppler moment estimation is presented after applying the IAA algorithm on simulated precipitation-like radar echoes. However, the ambiguous sidelobe suppression is highly dependent on the spectral width of the Doppler spectra.**

***Index Terms*—Doppler dealiasing, Non-uniform sampling, Log-periodic sampling, Periodic non-uniform sampling, Iterative Adaptive Approach (IAA), Precipitation, Weather Doppler spectra.**

I. Introduction

WEATHER radars use Doppler information from precipitation to detect the motion of hydrometeors. This helps identify the type of weather phenomenon (rain, snow, or hail) in the atmosphere. The three main Doppler parameters used to characterize weather are the total power in the reflected echo (zeroth Doppler moment), the mean Doppler frequency (1^{st} Doppler moment), and the Doppler spectral width (square root of the 2^{nd} Doppler moment around the mean frequency; i.e., the second central moment). These three parameters contribute to detecting the presence of hydrometeors, measuring the mean radial velocity and the velocity dispersion of the raindrops respectively. The Doppler spectrum of a typical precipitation-like weather target is continuous and wide. The Doppler spectral width characterizes the broadening of the spectrum which can be caused by many statistical effects, such as the turbulence in the precipitation, antenna beam shape, and the range weighting function (caused by the radar transmit waveform). In this paper, the broadening is assumed to be caused only by the turbulence.

Additionally, weather radars can only measure radial velocities up to a particular maximum unambiguous velocity in the directions towards and away from the radar, forming an observable velocity window. The original spectrum is folded back in the observation window for atmospheric phenomena having larger velocities than the unambiguous limit (due to storms, tornados, or turbulence). This folding (aliasing) affects the retrieval of the Doppler moments.

Aliasing can manifest in both range and Doppler velocity measurements. It depends on the radar's Pulse Repetition Frequency (PRF) or Sweep Repetition Frequency (SRF). Similar to the Nyquist limit in signal processing, the uniform sampling frequency (PRF or SRF) governs the observable limit. Furthermore, the unambiguous limit is a trade-off between the range and Doppler velocity domains.

The de-aliasing of the Doppler spectrum for precipitation-like targets is not a new problem and has been addressed in the literature. The techniques in literature can be categorized into pre-processing and post-processing techniques. Of these methods, four main techniques have been listed here - UNRAVEL algorithm, staggered PRF, wideband signals, and non-uniform sampling. Their approach and limitations are explained in the following sub-sections.

A. Post-processing algorithms

The post-processing algorithms use the retrieved Doppler moments as a function of space and time [1]–[4]. Typically, a detection algorithm is implemented by identifying the regions where aliasing takes place using multiple measurements of the Doppler moments in space [5]–[13]. While other methods use the evolution of the reflectivity fields in time (with multiple scans) as additional information to improve the performance [14]–[16]. The post-processing algorithms have the benefit of not compromising on the unambiguous range limit but suffer from the effects of corrupted or missing data.

The UNfold RAdar VELocity (UNRAVEL) algorithm is an open-source, modular algorithm [17] designed for Doppler velocity dealiasing within weather radar systems. It integrates supplementary results from reference points characterized by the least spectral power to iteratively enhance parameters [13]. Furthermore, the algorithm incorporates 3D continuity checks into its methodology. It consistently exhibited enhanced performance when compared to established dealiasing algorithms, including the 4DD algorithm [8], the unwrap algorithm [18],

978-83-956020-9-2 ©2024 Warsaw University of Technology
IRS-2024, Wrocław, Poland

the region-based algorithm implemented in Py-ART [19], and the multipass algorithm [6].

As the post-processing algorithms are applied on top of the Doppler spectrum with unambiguous limits, they are not studied in this paper. Additionally, the post-processing methods suffer in performance from the discontinuities in the received data.

B. Pre-processing techniques

1) Staggered PRF: The Staggered Pulse Repetition Frequency (PRF) approach involves utilizing multiple bursts of signal echoes, each alternating between high and low PRF [20]–[22]. The high PRF burst governs maximum unambiguous velocity limits, whereas low PRF burst determines the maximum unambiguous range, albeit with additional complexity in the signal processing stage. Unfortunately, in hardware-limited systems, attaining higher PRF is not achievable [23]. Moreover, the staggered PRF approach introduces numerous artifacts that adversely affect the spectral estimation [24].

2) Wideband signals: The narrowband ambiguity function displays recurring ambiguous lobes at regular intervals in both the range and velocity domains. On the contrary, the wideband ambiguity function showcases a prominent central lobe located at the actual Doppler velocity [25]. This main lobe is accompanied by various responses around ambiguous velocities, referred to as ambiguous sidelobes (these sidelobes do not possess the same power level as the main lobe). Since wideband systems require higher processing power and more complex systems, this method is not explored in this study.

3) Non-uniform sampling: In the context of uniform sampling, the sampling time (or frequency) remains constant, thereby establishing a fixed Nyquist limit. However, for non-uniform sampling, the Nyquist limit is found to be different. A particular form of non-uniform sampling, known as log-periodic sampling, has been addressed for the purpose of point spectral dealiasing [26]. This method was found to be the most promising with no constraint in hardware complexities (increase in PRF), thus there is no trade-off with the unambiguous interval in range.

The objective of this paper is to mitigate the aliasing phenomenon in the Doppler domain through the application of non-uniform sampling techniques within the signal processing framework. This enables enhanced detection and Doppler moment estimation. Furthermore, this does not compromise the maximum unambiguous range thereby proving to be an improvement over the state-of-the-art methods.

The main body of the paper is structured as follows. Section II explains the signal model of radar echoes in time from a precipitation-like extended target. Section III explains the theoretical considerations for non-uniform sampling. Section IV explains different types of non-uniform sampling considered in this paper and the radar echo simulation. Some results on simulated data are discussed in section V. The conclusions are presented in section VI.

II. Signal Model

The signal with extended Doppler velocity spectra is modelled based on [27]. The resultant signal takes the form of a complex exponential signal, incorporating the mean Doppler velocity and the Doppler spectral width as input parameters. The initial phase of this signal is uniformly distributed within the range of [-π,π]. The resulting signal model is given by,

$$s(t) = \sum_{m=1}^{M} a_m \exp\left[j\left(2\pi f_m t + \beta_m\right)\right] \tag{1}$$

where

$$a_m = a \quad \forall m$$

Here, $a_m = a = 1$ (i.e., the same amplitude for all scatterers is assumed). The input parameters are normalized to the maximum unambiguous velocity interval $(2 \times V_a)$. In the case of non-uniform sampling (explained in the later sections of the paper), they are normalized with the unambiguous velocity corresponding to the minimum sampling interval. The normalized Doppler frequencies f_m of all the scatterers are assumed to be *i.i.d* Gaussian distributed random variables with the normalized mean Doppler frequency μ_{fn} and variance (the square of the normalized Doppler frequency width) σ_{fn}^2. The distributions for both the Doppler frequency and phase are given by,

$$\begin{aligned} &\{f_m\}_{m=1}^{M} \overset{i.i.d.}{\sim} \mathcal{N}\left(\mu_{fn}, \sigma_{fn}^2\right), \\ &\{\beta_m\}_{m=1}^{M} \overset{i.i.d.}{\sim} \mathcal{U}[-\pi, \pi], \\ &\mu_{fn} = \mu_v/(2V_a), \\ &\sigma_{fn} = \sigma_v/(2V_a), \\ &V_a = \lambda/(4\Delta T_{\text{min}}), \end{aligned} \tag{2}$$

where ΔT_{min} is the minimum sampling time interval (minimum PRT), λ is the radar central wavelength, μ_v is the mean Doppler velocity, and σ_v is the Doppler velocity spectrum width.

A. Measurement Model

The measurement model in time consists of the signal model and an additive white complex Gaussian noise with variance σ_n^2. The overall measurement vector is given by,

$$\mathbf{z} = \mathbf{s} + \mathbf{n}, \qquad \{n_t\}_{t=0}^{T} \overset{i.i.d.}{\sim} \mathcal{CN}(0, \sigma_n^2), \tag{3}$$

where t denotes the time instance where we have the samples, T is the total Coherent Processing Interval (CPI), and $\mathbf{n}$ is the vector containing all the values of n_t. For simulation purposes, the noise variance(σ_n^2) is computed with a user-defined SNR value given as input [28].

III. Non-uniform sampling

Unlike the familiar uniform sampling spectral attributes, the non-uniform sampling spectrum possesses distinct characteristics [26]. Moreover, computing the spectrum of signals obtained through non-uniform sampling necessitates adjustments to conventional methods.

A. Non-uniform Nyquist limit

The aliasing in power spectrum for the uniform sampling case is denoted by the Nyquist sampling rate formula:

$$f_{\max} = f_s/2, \tag{4}$$

where $f_{\max}$ is the maximum observable frequency without aliasing and f_s is the sampling frequency. For the non-uniform sampling, there exists a Nyquist limit as mentioned in [29] which is governed by the time difference between the samples. This is given by the equation shown below,

$$t_i = t_0 + n_i p. \tag{5}$$

where t_0 is the first sample time, t_i is the i^{th} sample time and p is the greatest common factor such that each time difference Δt_i is an exact integer multiple (n_i) of p. Thus to determine the Nyquist limit for non-uniform sampling, one must identify the greatest factor p that satisfies,

$$f_{\text{Nyq}} = \frac{1}{2p} \tag{6}$$

where f_{Nyq} is the maximum observable frequency without aliasing using non-uniform sampling. The non-uniform Nyquist limit is thus given by (6). This definition of the maximum observable frequency also holds for uniform sampling case as in (4), where p is equal to the uniform sample spacing (which is equivalent to the inverse of f_s).

B. Special case- Irrational sample spacing

There exists a special case when the spacing between the samples is irrational. In such a scenario, there is no common factor p between the sample spacing; thus, there is no theoretical Nyquist limit. Unfortunately, this holds only for an ideal case where the time samples can be measured with infinite precision. For a real-life system that only records the time stamp of samples accurately to D decimal places, a more realistic Nyquist limit exists given by,

$$f_{\text{Nyq}} \leq \frac{1}{2}10^D. \tag{7}$$

Intuitively, if the radar is only capable of measuring received echo with one micro-second precision, then the largest common factor between irrational sampling times would be one micro-second. Thus, for the practical irrational sampling space case, (6) and (7) are essentially the same.

IV. Simulation with Non-uniform Sampling

A. Log-periodic sampling

In log-periodic sampling, which is a type of non-uniform sampling, the sample time increments exponentially change with each sample (radar echo), i.e., the logarithm of the sample spacing is periodic [26]. Here, the individual sample times are given by

$$g(z) = (T/N)(b/a)\left[e^{az} - 1\right], \tag{8}$$

where b is the minimum sample spacing factor that is chosen to fit $\Delta T_{\min}$, a is the exponential growth rate of the sample time differences, and N is the total number of samples (pulses or sweeps). The parameters b, a, and N should be chosen such that the overall time occupied by the radar echo samples must satisfy the maximum Coherent Processing Interval (CPI) that is allowed within the burst, this is denoted by T.

B. Periodic Non-uniform sampling

Periodic Non-Uniform (PNU) sampling refers to the practice of sampling a signal at intervals that are unevenly spaced but still recurrent within a specific period [30], [31]. PNU sampling bears a resemblance to the multi-burst processing technique in radar systems, wherein each burst consists of a collection of non-uniform samples. Within each burst, the sampling arrangement can be selected from a variety of non-uniform sampling schemes. Notably, log-periodic sampling has demonstrated superior performance compared to various other non-uniform sampling methods [32] so log-periodic sampling is used. The effectiveness of PNU log-periodic sampling is assessed using the optimized values of b, a, and N, with each burst duration serving as the maximum CPI denoted by the time period (T).

In scenarios involving fast-scanning weather radars, the time on target is constrained, resulting in a small T. In these circumstances, although we have less time on target for a single scan, it becomes feasible to aggregate reflected echoes from multiple scans using PNU sampling. This can be done by having an inter-burst spacing equal to the scan-to-scan time of the radar. It should be noted that inter-burst spacing might introduce periodicity effects similar to a convolution of the signal with a rectangular pulse signal. The resulting spectral performance of the coherent bursts surpasses that of a single burst scenario.

To enhance the SNR of the signal, an Iterative Adaptive Approach (IAA) Algorithm is used. This is a non-parametric and hyperparameter-free, weighted least-squares-based iterative algorithm to suppress the noise in the signal [33] [34]. Each burst within the multi-burst PNU log-periodic sampling setup can be transformed into a single signal snapshot for the Iterative Adaptive Approach (IAA) algorithm. This algorithm, initially intended for source localization, has been adapted for spectral estimation. There is an inherent resemblance between these two domains, and the signal-processing methodologies are analogous. Given that IAA operates through an iterative process, the duration for achieving convergence tends to increase, as it relies on the number of iterations needed. The time consumed for each iteration predominantly arises from the computation of the inverse matrix R^{-1}, a square matrix with dimensions $N \times N$, where N represents the total count of samples (pulses/sweeps) within a burst. Additionally, the computation time is dependent on the quantity of signal snapshots used for estimating the covariance matrix.

V. Results and Discussion

A comparative simulation is done between uniform and non-uniform sampled signals. The CPI of the radar is taken to be 0.8 seconds. For the uniform sampling case, this amounts to a total number of 800 samples with 1 millisecond spacing.

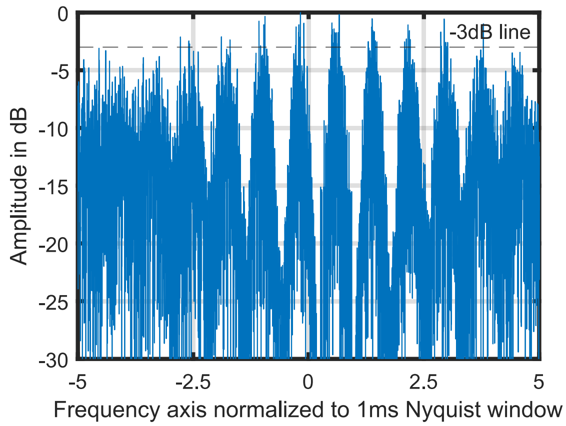

Fig. 1. Extended Doppler spectrum $\mu_{fn} = 0.6$, and $\sigma_{fn} = 0.1$. Log-periodic sampling with N = 638, b = 0.85813899, a = 0.000472337 with T = 0.8 seconds.

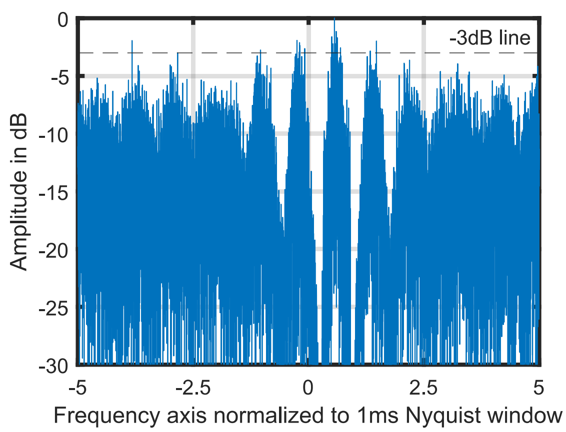

Fig. 2. Extended Doppler spectrum with $\mu_{fn} = 0.6$, and $\sigma_{fn} = 0.1$. PNU '$3T$ inter-burst spacing' with N = 638, b = 0.85813899, a = 0.000472337 with T = 0.8 seconds for six burst case ($18T$ in total).

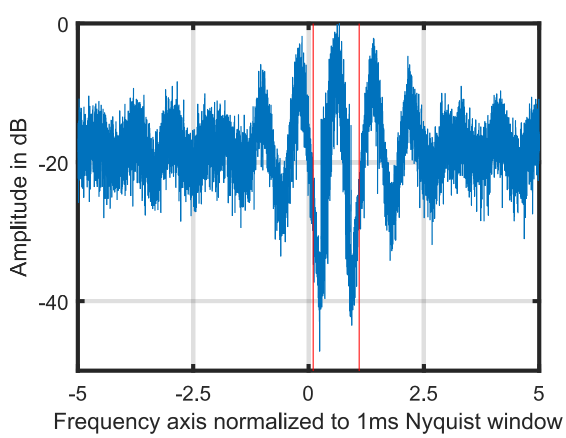

Fig. 3. Extended Doppler spectrum of PNU '$3T$ inter-burst spacing' with $\mu_{fn} = 0.6$, and $\sigma_{fn} = 0.1$ after 10 IAA iterations.

Since the non-uniform samples are considered to be with micro-second precision, the use of a milli-second time axis becomes inapplicable. An example of the non-uniform time vector (for the Log-periodic sampling) of the useful samples can be represented as:

$$\mathbf{t} = [1.008, 2.050, 3.132, \cdots, 799.231] \quad ms \tag{9}$$

Thus the use of a micro-second time axis makes more sense with D = 6 from (7). Since the 1 ms minimum sample spacing is also respected in this case, the total number of useful samples is less than 800.

The power spectrum of log-periodic sampling for 1000 scatterers with normalized Doppler spectrum width of $\sigma_{fn} = 0.01$ is shown in Fig.1. The input parameters are normalized with the unambiguous Doppler velocity corresponding to the uniform one-millisecond sampling case. Here, the ambiguous sidelobe levels are quite high for extended Doppler spectral widths with multiple scatterers despite no noise being added to the signal. The actual Doppler spectrum is thus found to be ambiguous.

A spectral comparison between the log-periodic sampling and PNU '$3T$ inter-burst' spacing sampling can be made with Fig. 1 and Fig. 2, respectively. It can be seen that a 6-burst PNU with $3T$ inter-burst spacing performs better than the log-periodic case (equivalent to 1-burst PNU) by having reduced sidelobe levels and a distinguishable main lobe. Additionally, when ten iterations of the IAA algorithm are done, the spectral noise is more suppressed, showing a clear spectral structure as seen in Fig. 3.

The performance of the PNU waveform structure, coupled with the IAA algorithm, is assessed through theoretical simulation. A Monte Carlo simulation encompassing input SNR values, burst counts, IAA iterations, and Doppler widths is done. The Doppler moments, crucial for target characterization, can be determined utilizing the equations established in [35]. These equations for moments estimation are inherently formulated for uniform sampling, ensuring calculations encompass the complete $2V_a$ window devoid of ambiguities.

For the case of uniform sampling, the moments are estimated over the complete unambiguous observable frequency window ($2V_a$). To extend these equations for non-uniform sampling, the frequency window used for moments estimation is still maintained as $2V_a$, though the unambiguous observable frequency range is extended by 1000 times (by the use of micro-second precision over milli-second spacing). The estimation window is fixed by identifying the spectrum's peak over the entire range and utilizing that point as the center point for a window ranging $2V_a$. Subsequently, the Doppler moments are estimated within this window as shown by the red vertical lines in Fig. 3.

A. Mean Doppler spectral estimation

Based on observations involving multiple Doppler spectral widths, it can be inferred that the occurrence of false peaks becomes more noticeable with broader spectral widths ($\sigma_{fn} > 0.1$). This phenomenon is due to ambiguous sidelobes with

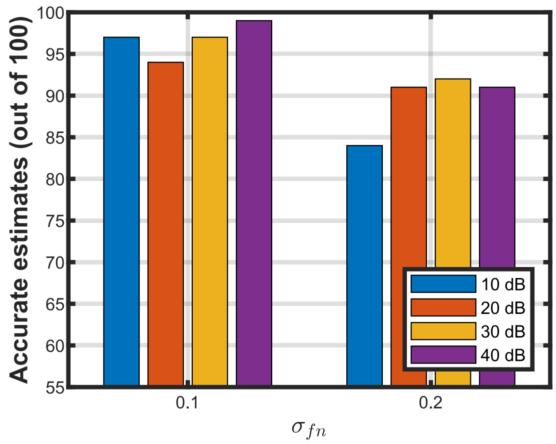

Fig. 4. Graph showing the number of accurate Doppler mean estimations (out of 100) after 10 IAA iterations for different input SNR values and two different Doppler spectral width values for a six-burst PNU case.

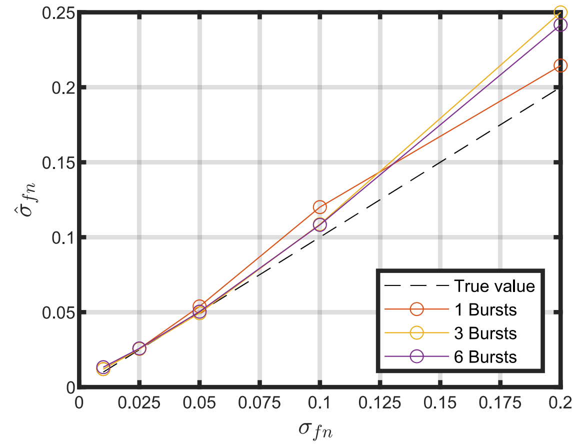

Fig. 5. Estimated vs True normalized spectral width for different bursts for 30 dB input SNR for PNU sampling after 10 IAA iterations.

higher spectral power where suppression of such artifacts is difficult. These false peaks impact the positioning of the one-millisecond Nyquist window and consequently influence the mean estimation.

Hence, for low Signal-to-Noise Ratio (SNR) signals with extended Doppler spectral widths, a constraint is introduced where the estimated normalized mean Doppler velocity is ensured to be within a specific spectral interval around the true normalized mean Doppler velocity (the interval is a function of the true normalized spectral width). For $\sigma_{fn} \leq 1$, when the estimated mean falls within the intervals of (-$0.5\sigma_{fn}$,$0.5\sigma_{fn}$) from the actual mean, it is considered to be an accurate estimation. And for higher values of σ_{fn} if the mean estimation is within (-$0.75\sigma_{fn}$,$0.75\sigma_{fn}$) from the actual mean, this is considered as an accurate estimation.

The distribution of accurate estimates for various spectral widths and input Signal-to-Noise Ratio (SNR) values are shown in Fig. 4. As anticipated, Fig. 4 shows better estimation for scenarios with reduced noise levels and signals with narrower Doppler spectral widths. Moreover, the improvement in performance due to an increase in the number of bursts (number of snapshots for the IAA algorithm) is also confirmed by multiple trials.

B. Doppler spectral width estimation

The comparison between estimated and true spectral widths for various input SNR values is illustrated in Fig. 5.

As depicted in Fig. 5, it becomes apparent that narrower Doppler spectral width ($\sigma_{fn} \leq 1$) are estimated with greater accuracy in cases involving 3 bursts and 6 bursts, as opposed to the 1-burst scenario. Given that the Doppler spectral width for typical meteorological phenomenon falls within the range of $\frac{1}{20}th$ to $\frac{1}{30}th$ of the $1ms$ Nyquist window size [36], employing multiple bursts is advantageous for such scenarios. Furthermore, to illustrate the impact of multiple bursts, Fig. 5 showcases the estimated versus true spectral width for varying numbers of bursts in the context of a 30 dB input SNR.

From the simulations, for the case of lower Doppler widths, as the number of bursts in PNU processing is higher, the Doppler spectral width estimation becomes more accurate. The estimation performance is better when the noise is lower. Additionally, the estimation performance for PNU after 10 IAA iterations is comparable to the estimation performance of uniform sampling.

VI. Conclusion

The Nyquist limit in the context of non-uniform sampling has been validated. The process of modeling the signal to meet a specific unambiguous Doppler velocity requirement (beyond the uniform sampling limit) has been outlined. It is shown that by using non-uniform sampling techniques it is possible to extend the unambiguous Doppler window by several orders depending on the measurement time accuracy of the received signals. In log-periodic sampling, the sample times and the resultant power spectrum are dependent upon four parameters: the number of samples (N), the exponential growth factor (a), the minimum sample spacing factor (b), and the maximum Coherent Processing Interval (T). Through testing optimized values for different Doppler spectral widths, it has been determined that the optimization performance remains consistent and unaffected by the Doppler spectral width. By using the IAA Algorithm, it is proven that dealiasing with narrow Doppler spectral width is possible with exceptional performance.

In the case of a fast-scanning radar, boosting the spectral estimation performance by extending the Coherent Processing Interval (CPI) is impractical. Instead, a solution has been found by utilizing multi-scan data and implementing a non-uniform sampling strategy known as 'Periodic Non-Uniform (PNU)' sampling. This approach has effectively eliminated the necessity for a higher CPI. Multi-snapshot IAA algorithm has been used for this case where each burst is treated as a snapshot, and the noise covariance matrix is collectively estimated. This technique substantially enhances performance, surpassing the results achieved with a single burst of optimized log-periodic sampling.

Monte Carlo simulations have been conducted encompassing a range of Doppler spectral widths, distinct input SNR levels for random noise, and varying numbers of bursts. The outcomes of these simulations align consistently with the theoretical expectations and conclusions drawn from the study. It is found that the accuracy of Doppler spectral width estimation in PNU sampling improves with a higher number of bursts, particularly for lower Doppler widths. This estimation performance is further enhanced when noise levels are lower. Furthermore, the estimation performance achieved in PNU sampling is comparable to that observed in the case of uniform sampling with the added benefit of Doppler dealiasing.

VII. Acknowledgements

This study was part of the thesis collaboration between TU Delft and Robin radar systems. The authors would like to thank Dr.Nikita Petrov for his assistance with the Iterative Adaptive Approach (IAA) algorithm.

References

[1] Y. Yamada and M. Chong, "Vad-Based Determination of the Nyquist Internal Number of Doppler Velocity Aliasing without Wind Information," *Journal of the Meteorological Society of Japan*, vol. 77, no. 2, pp. 447–457, 1999.

[2] P. Tabary and G. Scialom, "Real-Time Retrieval of the Wind from Aliased Velocities Measured by Doppler Radars," *Journal of Atmospheric and Oceanic Technology*, vol. 18, no. 6, pp. 875–882, 2001.

[3] J. Gong, L. Wang, and Q. Xu, "A Three-Step Dealiasing Method for Doppler Velocity Data Quality Control," *Journal of Atmospheric and Oceanic Technology*, vol. 20, no. 12, pp. 1738–1748, 2003.

[4] Z. Jing and G. Wiener, "Two-Dimensional Dealiasing of Doppler Velocities," *Journal of Atmospheric and Oceanic Technology*, vol. 10, no. 6, pp. 798–808, 1993.

[5] Ray P. S. and C. Ziegler, "De-Aliasing First-Moment Doppler Estimates," *Journal of Applied Meteorology and Climatology*, vol. 16, no. 5, pp. 563–564, 1977.

[6] J. Zhang and S. Wang, "An Automated 2D Multipass Doppler Radar Velocity Dealiasing Scheme," *Journal of Atmospheric and Oceanic Technology*, vol. 23, no. 9, pp. 1239 – 1248, 2006.

[7] W. R. Bergen and S. C. Albers, "Two- and Three-Dimensional Dealiasing of Doppler Radar Velocities," *Journal of Atmospheric and Oceanic Technology*, vol. 5, no. 2, pp. 305–319, 1988.

[8] C. N. James and R. A. Houze, "A Real-Time Four-Dimensional Doppler Dealiasing Scheme," *Journal of Atmospheric and Oceanic Technology*, vol. 18, no. 10, pp. 1674–1683, 2001.

[9] E. Lim and J. Sun, "A Velocity dealiasing technique using rapidly updated analysis from a four-dimensional variational doppler radar data assimilation system," *Journal of Atmospheric and Oceanic Technology*, vol. 27, no. 7, pp. 1140–1152, 7 2010.

[10] Elits M and Smith S, "Efficient Dealiasing of Doppler Velocities Using Local Environment Constraints," *Journal of Atmospheric and Oceanic Technology*, vol. 7, no. 1, pp. 118–128, 1990.

[11] G. Li, G. He, X. Zou, and P. S. Ray, "A velocity dealiasing scheme for C-band weather radar systems," *Advances in Atmospheric Sciences*, vol. 31, no. 1, pp. 17–26, 1 2014.

[12] Q. Xu and K. Nai, "Mesocyclone-targeted doppler velocity dealiasing," *Journal of Atmospheric and Oceanic Technology*, vol. 34, no. 4, pp. 841–853, 4 2017.

[13] G. He, G. Li, X. Zou, and P. S. Ray, "A velocity dealiasing scheme for synthetic C-band data from China's new generation weather radar system (CINRAD)," *Journal of Atmospheric and Oceanic Technology*, vol. 29, no. 9, pp. 1263–1274, 9 2012.

[14] M. Wüest, "Dealiasing Wind Information from Doppler Radar for Operational Use," Swiss Federal Institute of Technology, Zurich, Tech. Rep., 2001.

[15] B. E. Mapes, "Doppler Radar Observations of Mesoscale Wind Divergence in Regions of Tropical Convection," Tech. Rep., 2005.

[16] H. Yamauchi, O. Suzuki, and K. Akaeda, "Yamauchi et al., A Hybrid Multi-PRI Method to Dealias Doppler Velocities," *SOLA*, vol. 2, pp. 92–95, 2006. [Online]. Available: http://www.jstage.jst.go.jp/browse/sola/

[17] V. Louf, A. Protat, R. C. Jackson, S. M. Collis, and J. Helmus, "Unravel: A robust modular velocity dealiasing technique for doppler radar," *Journal of Atmospheric and Oceanic Technology*, vol. 37, no. 5, pp. 741–758, 5 2020.

[18] D. R. Burton, M. A. Herráez, M. A. Gdeisat, and M. J. Lalor, "Fast two-dimensional phase-unwrapping algorithm based on sorting by reliability following a noncontinuous path," *Applied Optics, Vol. 41, Issue 35, pp. 7437-7444*, vol. 41, no. 35, pp. 7437–7444, 12 2002. [Online]. Available: https://opg.optica.org/viewmedia.cfm?uri=ao-41-35-7437seq=0html=true https://opg.optica.org/abstract.cfm?uri=ao-41-35-7437 https://opg.optica.org/ao/abstract.cfm?uri=ao-41-35-7437

[19] J. J. Helmus and S. M. Collis, "The Python ARM Radar Toolkit (Py-ART), a Library for Working with Weather Radar Data in the Python Programming Language," *Journal of Open Research Software*, vol. 4, no. 1, p. 25, 7 2016.

[20] M. Skolnik, *Radar Handbook - 3rd Edition*. McGraw Hill, 2008.

[21] G. Galati, *Advanced radar techniques and systems*. Institution of Electrical Engineers, 1993.

[22] D. C. Schleher, "MTI and pulsed doppler radar with MATLAB / D. Curtis Schleher." Boston, 2010.

[23] C. Alabaster, *Pulse Doppler Radar: Principles, technology, applications*, ser. Radar, Sonar and Navigation. Institution of Engineering and Technology, 2012. [Online]. Available: https://digital-library.theiet.org/content/books/ra/sbra024e

[24] G. M. Cleetus, "Properties of Staggered PRF Radar Spectral Components," *IEEE Transactions on Aerospace and Electronic Systems*, vol. AES-12, no. 6, pp. 800–803, 1976.

[25] D. Swick, "A Review of Wideband Ambiguity Functions," Naval Research Laboratory, Washington, D.C, Tech. Rep., 1969.

[26] J. T. VanderPlas, "Understanding the Lomb–Scargle Periodogram," *The Astrophysical Journal Supplement Series*, vol. 236, no. 1, p. 16, 5 2018.

[27] T. Dash, O. A. Krasnov, and A. G. Yarovoy, "Performance Analysis of the Wind Field Estimation for a Very Fast Scanning Weather Radar," in *2022 23rd International Radar Symposium (IRS)*, vol. 2022-September. IEEE, 9 2022, pp. 420–425. [Online]. Available: https://ieeexplore.ieee.org/document/9905006/

[28] D. S. Zrnić, "Simulation of Weatherlike Doppler Spectra and Signals," *Journal of Applied Meteorology and Climatology*, vol. 14, no. 4, pp. 619–620, 6 1975.

[29] L. Eyer and P. Bartholdi, "Variable stars: Which Nyquist frequency?" *Astronomy and Astrophysics Supplement Series*, vol. 135, no. 1, pp. 1–3, 2 1999. [Online]. Available: https://aas.aanda.org/articles/aas/abs/1999/04/ds1574/ds1574.html

[30] R. H. Kestur, "Application of periodic nonuniform sampling for detection of radar signals," Ph.D. dissertation, Texas A&M University-Kingsville, 2017.

[31] S. Zhao, R. Wang, Y. Deng, Z. Zhang, N. Li, L. Guo, and W. Wang, "Modifications on Multichannel Reconstruction Algorithm for SAR Processing Based on Periodic Nonuniform Sampling Theory and Nonuniform Fast Fourier Transform," *IEEE Journal of Selected Topics in Applied Earth Observations and Remote Sensing*, vol. 8, no. 11, pp. 4998–5006, 11 2015.

[32] A. W. Doerry, "Radar Doppler processing with nonuniform PRF," Tech. Rep., 2017. [Online]. Available: https://www.osti.gov/biblio/1373645

[33] T. Yardibi, J. Li, P. Stoica, M. Xue, and A. B. Baggeroer, "Source localization and sensing: a nonparametric iterative adaptive approach based on weighted least squares," *IEEE Transactions on Aerospace and Electronic Systems*, vol. 46, no. 1, pp. 425–443, 1 2010.

[34] N. Petrov, "Migrating Target Detection in Wideband Radars," Ph.D. dissertation, 2019. [Online]. Available: https://doi.org/10.4233/uuid:08556a7c-ef90-43f7-998b-f103ceea6267

[35] R. J. Doviak and D. S. Zrnic, *Doppler radar and weather observations*. Academic Press, 1993.

[36] R. J. Doviak, D. S. Zrnic, and D. S. Sirmans, "Doppler Weather Radar," *Proceedings of the IEEE*, vol. 67, no. 11, pp. 1522–1553, 1979.